Experimental Validation of the Adiabatic Assumption of Short-Circuit Tests on Bare Conductors

Jordi-Roger Riba, David González, Pau Bas-Calopa, and Manuel Moreno-Eguilaz

Abstract— **According to various international standards, many high-voltage devices must withstand short-circuit tests. Due to the enormous power and current requirements, they have to be tested in very specialized and expensive power laboratories, which are scarce and not affordable for the vast majority of electrical product manufacturers. It is proposed to break the time limit of about one second imposed by the standards by using a lower current to heat for a longer time, requiring more affordable equipment and thus reducing the cost for testing. This work analyzes the limits of the adiabatic assumption in short-circuit tests in order to quantify how the duration of these tests can be extended to reduce the power required and the current applied, while obtaining almost the same results, i.e., the same temperature at the end of the heating phase of the tests. For this purpose, bare cylindrical conductors are analyzed and the temperature dependence of the properties of the conductor material is considered. Experimental and simulation results presented in this paper suggest that by applying this approach, short-circuit tests intended for product design, verification and quality control can be performed in much less demanding and affordable laboratory facilities.**

Index Terms— **adiabatic, finite element method, short-circuit, simulation, temperature rise, thermal model, tests**

I. INTRODUCTION

P OWER systems are experiencing a steady growth worldwide, thus leading to an increase in short-circuit levels [1]–[3]. Short-circuits are among the most common fault modes in electrical networks, and are complex electromagnetic transient phenomena that have received much attention in the scientific field [4]. Short-circuits are considered damaging fault modes, because they can cause severe thermal and mechanical stress on the components involved [5], [6], thus increasing the risk of power system failure [7]. Because of their damaging effects, electrical protections must clear short-circuit faults as quickly as possible. However, electrical protection devices take some time to clear short-circuits, tend to generate particularly high temperatures [8] and have the potential to produce powerful faults [9], so electrical protections play a critical role in ensuring that short-circuit currents do not cause irreversible damage to the electrical equipment involved.

It is essential to test electrical components to ensure that fault currents do not compromise their safety limits. By limiting the temperature rise during the short-circuit condition, the life of the equipment involved is usually increased [10].

Short-circuit tests are often referred to in the international standards such as the IEC 60909 [11], the IEC 62271-1 [12], the IEC-60694 [13], the ANSI C37.51a [14] or the IEEE Std. C37.20.1 [15] as short-time withstand current test and peak withstand current test. Electrical equipment such as substation connectors, conductors, control gear, switchgear, or power transformers among others, must be tested and certified according to such standards. Most electrical equipment is required to endure short-time withstand currents in the kiloampere range, typically from a few kiloamperes to several tens of kiloamperes [2], usually for a duration of 1 s, although other durations are allowed depending on the standard. For example the IEC 62271-1 standard [12] allows the duration to be extended up to 5 s under certain circumstances.

It is important to have a thorough knowledge of the dynamics of the short-circuit and to develop accurate mathematical tools to predict the temperature rise during the short-circuit, as this can lead to better designs of the equipment involved [16]. Short-circuit analysis is therefore a fundamental tool for determining the thermal rating of electrical equipment [17] and ensuring that it can withstand such harsh conditions without suffering irreversible damage or significant reduction in lifetime [2].

Short-circuit tests and high-current busbars have been widely simulated using finite element simulations [18]–[21] although in some cases, particularly for cylindrical, very accurate results can be obtained by solving analytical equations [22], [23], which are often simpler and faster to use.

Due to its short duration, adiabatic conditions are often assumed during the heating phase of the short-circuit [24].

J.-R. Riba is with the Electrical Engineering Department of the Universitat Politècnica de Catalunya, 08222 Terrassa, Barcelona, Spain (e-mail: jordi.riba-ruiz@upc.edu).

D. González is with SBI Connectors, 08635 Sant Esteve Sesrovires, Barcelona, Spain (e-mail: david.gonzalez@sbiconnect.es).

M. Moreno-Eguilaz is with the Electronics Engineering Department of the Universitat Politècnica de Catalunya, 08222 Terrassa, Barcelona, Spain (e-mail: manuel.moreno.eguilaz@upc.edu).

P. Bas-Calopa is with the Electrical Engineering Department of the Universitat Politècnica de Catalunya, 08222 Terrassa, Barcelona, Spain (e-mail: p.bas@upc.edu).

Thus, it is generally accepted that the adiabatic criterion can only be applied if the heating phase lasts for a short time [21], but there are no specific rules to define this "short time". This paper focuses on this aspect because if the adiabatic assumption could be applied to longer duration short-circuits, it would simplify the energy and material requirements of the expensive facilities needed to perform such tests. Because of the huge instantaneous power requirements and the short duration of the current delivered [25], short-circuit tests must be carried out in very expensive and select power laboratories, which are beyond the reach of the vast majority of manufacturers of electrical products. This means that customers often have to wait a long time for their products to be tested, the tests are expensive and are carried out by technicians from the external laboratory, so the testing expertise does not remain with the manufacturer's staff. However, if the adiabatic approach can be applied for a longer time, the short-circuit duration can be extended, drastically reducing both the current and the instantaneous power required for the test. For example, if the short-circuit duration can be extended from 1 s to 25 s, since the power requirement is almost proportional to I^2R, the current level can be reduced by about 5 times, while the instantaneous power can be reduced by about 25 times. This means that such tests can be performed in a much less demanding and much more affordable laboratory.

This paper focuses on this topic by experimentally studying the thermal behavior of a cylindrical copper conductor and corroborating the results with software tools programmed by the authors of this work which, by solving the non-steady state heat balance equation, reproduce the thermal behavior of the conductor during both the heating and cooling phases of the short-circuit test. From the results obtained, the duration of the short-circuit that can be considered as adiabatic is derived and the necessary corrections are proposed. To the best of the authors' knowledge, there are no articles dealing on this aspect.

II. TRANSIENT THERMAL MODEL OF THE CONDUCTOR

The temperature of a bare conductor depends on the self-generated Joule heating and the external ambient temperature. As current flows through the metallic conductor material, usually copper or aluminum, heat flows from the conductor through the air.

The short-circuit current has a transient behavior, i.e., the current is not constant during the fault condition. This paper deals with the root-mean-square (RMS) value of the current during the duration of the short-circuit test because it is suggested by international standards such as the IEC 62271-1 [12]. It is also suggested that the nominal duration of the short-circuit be set at 1 s, although 0.5 s, 2 s and 3 s are also acceptable.

Although short-circuits produce a brief but intense mechanical stress, this stress is not evaluated in this paper because it requires different approaches and because the mechanical stress in cylindrical conductors and busbars is often limited [26]. In addition, conductors have to undergo various standard mechanical tests (stress-strain test, ultimate breaking load test, breaking load of individual wires, stress-strain test, load test, breaking load of individual wires, stress-strain test,

ductility, etc.) which are more demanding from a mechanical point of view than the short circuit condition.

A. Non-steady state heat balance equations

Both the IEEE Std. 738 [22] and CIGRE [23] develop the non-steady-state heat balance equation for a bare conductor,

$$I_{RMS}^2 R(T) = P_c + P_r - P_s + mc_p(T)\frac{dT}{dt} \quad \text{[W/m]} \tag{1}$$

I [A] being the RMS value of the short-circuit current, R [Ohm/m] the resistance of the conductor per unit length, P_c [W/m] and P_r [W/m] are the heat loss terms per unit length due to convective and radiative cooling, respectively, P_s [W/m] is the solar heat gain term per unit length, m [kg/m] the mass of the conductor per unit length, $c_p(T)$ [J/(kgK)] the specific heat capacity of the conductor material and T [K] the absolute average conductor temperature.

The temperature dependence of the resistance is given by,

$$R(T) = R_{T_0}[1 + \alpha(T - T_0)] \tag{2}$$

T_0 [K] being a reference temperature, usually 293.15 K, i.e., 20 ºC, T [K] the average temperature of the conductor and α [K^{-1}] is the temperature coefficient of the resistance.

In indoor conditions, where there is no rate of heat gain from the sun,

$$I_{RMS}^2 R(T) = P_c + P_r + mc_p(T)\frac{dT}{dt} \quad \text{[W/m]} \tag{3}$$

Assuming natural convection (still air), the heat loss term per unit length due to convective cooling can be expressed as [22],

$$P_c = h\pi D(T - T_{air}) \quad \text{[W/m]} \tag{4}$$

where D is the diameter of the conductor. According to [22], the heat transfer coefficient can be calculated as,

$$h = \frac{3.645}{\pi}\rho_{air}^{0.5} D^{-0.25}(T - T_{air})^{0.25} \quad \text{[W/(m}^2\text{K)]} \tag{5}$$

Radiative heat loss per unit length can be expressed as [22],

$$P_r = \varepsilon\sigma\pi D(T^4 - T_{air}^4) \quad \text{[W/m]} \tag{6}$$

where $\sigma = 5.67 \cdot 10^{-8}$ W/(m^{2}K^4) is the Stefan-Boltzmann constant, and ε is the emissivity coefficient, which is assumed to be 0.5 [27], [28].

According to the IEEE 738 Std. [22], the density of air depends on the elevation of the conductor H [m] above sea level and the temperature of the air in the boundary layer of the conductor as,

$$\rho_{air} = \frac{1.293 - 1.525 \cdot 10^{-4}H + 6.379 \cdot 10^{-9}H^2}{1 + 0.00367(T_{air} + T)/2}dt \quad \text{[kg/m}^3\text{]} \tag{7}$$

T_{air} [K] being the absolute ambient air temperature.

Equation (3) can be solved iteratively by calculating the incremental temperature at each time step as,

$$dT = \frac{I_{RMS}^2 R(T) - P_c - P_r}{mc_p(T)}dt \quad \text{[K]} \tag{8}$$

By integrating (8) between $t = 0$ and any arbitrary time t in time steps $\Delta t = t_{i+1} - t_i$ from $T = T_{initial}$ (initial conductor temperature), it is not difficult to find the evolution of the conductor temperature with time,

$$T_{i+1} = T_i + \frac{I_{RMS}^2 R(T_i) - P_{c,t_i} - P_{r,t_i}}{mc_p(T_i)}(t_{i+1} - t_i) \quad \text{[K]} \tag{9}$$

Note that (9) applies to both phases of the short-circuit. During the heating phase ($0 \leq t_i \leq t_{sc}$) the term $I^2_{RMS}R(T_i)$ applies. At the end of the short-circuit, i.e., when $t_i = t_{sc}$, the conductor reaches its maximum temperature $T_i = T_{max}$. For $t_i > t_{sc}$ the current is zero and the temperature of the conductor cools down. It is worth noting that T_{max} is an important parameter extracted from the short-circuit, which can be used to determine whether or not the sample under test has passed the standard short-circuit test.

B. Non-steady state heat balance equations under adiabatic conditions

Short circuits usually last a short time due to the inherent delay of the protection devices. Therefore, the duration of standard short-circuit tests is usually very short, ranging from less than a second to a few seconds. For example, according to the IEC 60909-0 standard [11], which describes the characteristics of short-circuit currents in three-phase alternating current systems, the rated duration of short-circuit tests is 0.5 s or more, which is similar to the preferred duration suggested by the IEC 62271-1 [12], which is 1 s, although durations of 0.5 s, 2 s, and 3 s are also allowed. These short times allow the adiabatic assumption to be applied with great accuracy to determine the final temperature reached by the test object during the short-circuit test, as will be shown below.

Under adiabatic conditions, i.e., when there is no heat or mass transfer between the conductor and the environment, $P_c = P_r = 0$. When applying the adiabatic approach, it is assumed that the heat generated during the short-circuit due to the Joule losses is completely used to raise the temperature of the test object, so that (8) can be expressed as,

$$dT = \frac{I^2_{RMS}R(T)_s}{mc_p(T)} dt = \frac{I^2_{RMS}R_{T_0}[1+\alpha(T-T_0)]}{mc_p(T)} dt \qquad (10)$$

From (10), it results,

$$T_{i+1} = T_i + \frac{I^2_{RMS}R(T_i)}{mc_p(T_i)}(t_{i+1} - t_i) \qquad (11)$$

Thus, by iterating from $t = 0$ to $t = t_{sc}$ (short-circuit duration) in time steps $\Delta t = t_{i+1} - t_i$ from $T = T_{initial}$, it is not difficult to find the final conductor temperature T_{max} at the end of the short-circuit duration. It should be noted that equations (9) and (11) have been solved using Matlab® scripts written by the authors of this work.

III. FEM SIMULATION OF THE TRANSIENT THERMAL MODEL OF THE CONDUCTOR

The method described in Section II applies only to cylindrical conductors or elements with cylindrical geometry. However, short-circuit tests can be applied to electrical products with more complex geometry, where the method based on the solution of (9) cannot be applied because it assumes a cylindrical geometry. In such cases FEM simulations are a good alternative [18], although they are more time consuming and require more intensive computational resources.

In this paper a multiphysics three-dimensional FEM model based on the equations detailed in Section II is built in the Comsol® Multiphysics environment, as an alternative and internationally recognized method to evaluate the accuracy of the equations detailed in Section II. Although FEM is used in this paper as a verification method in a standard cylindrical problem, this is only a starting point. In the case of complex geometries, FEM is a valuable method for obtaining an accurate solution. The three-dimensional tetrahedral mesh applied to the studied conductor geometry consists of 1530938 tetrahedral elements, 228160 triangular elements, and 12800 edge elements.

Resistive or Joule losses are the heat source of the FEM model, providing the link between the thermal and electromagnetic physics. The applied heat loss terms due to natural convection and radiation are as (4) and (6), respectively.

Fig. 1 shows the mesh applied to the analyzed three-dimensional FEM model of the conductor.
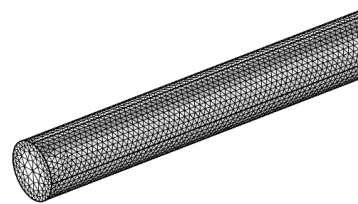

Fig. 1. Mesh applied to the analyzed three-dimensional FEM model of the conductor.

IV. EXPERIMENTAL TESTS

A. Experimental setup

Several experimental short-circuit tests were carried out in the AMBER high-voltage laboratory of the Universitat Politècnica de Catalunya. For this purpose, a high-current transformer (max output voltage 10 V, max output current 14 kA_peak) was used. It allows both the output voltage and current to be regulated, as well as the short-circuit duration. The output terminals of the high-current transformer were connected directly to the conductor loop, as shown in Fig. 2.
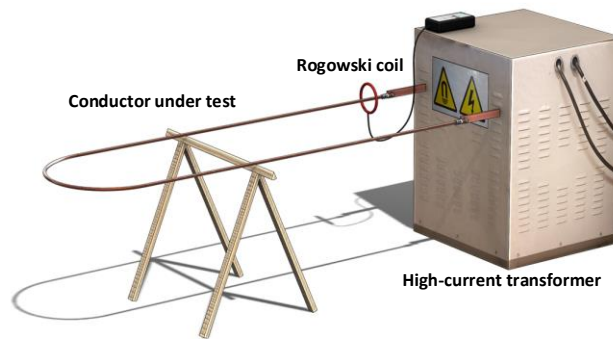

Fig. 2. Experimental setup used in the AMBER high-voltage laboratory.

The output current of the transformer was measured using a calibrated Rogowski coil (CWT300, 0.1 mV/A, ±1%, $I_{max,peak}$ = 60 kA, PEM Ltd., Nottingham, UK) at a rate of 2500 samples/s. Temperature measurements were made using 0.2 mm diameter welded-tip T-type thermocouples (temperature range from −75 to + 400°C) placed in the central strands of the copper conductor. Readings from the thermocouples were acquired every 100 ms using an OMEGA DAQ USB-2400 acquisition

card. Experimental tests were performed under atmospheric conditions at 12 ºC. Tests were performed by applying short-circuit currents between 5700 and 6300 A$_{RMS}$.

Fig. 3 shows the current waveform during a 2 s short-circuit. It can be seen that the short-circuit current decreases with time due to the increase in conductor resistance caused by the temperature rise during the heating phase of the short-circuit.
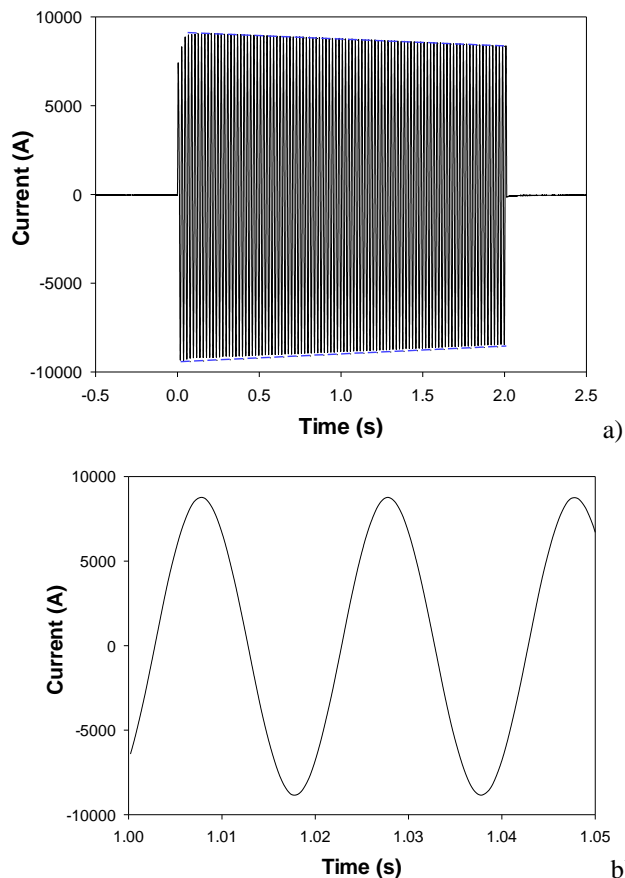

Fig. 3. a) Current evolution during a short-circuit test of 2 s duration. b) Detail of the 50 Hz current waveform in the 1.00 – 1.05 s range.

It should be noted that the ambient temperature was kept constant during the short-circuit test. Prior to the tests, it was ensured that the test conductor was at room temperature. The short-circuit tests were carried out on a bare stranded copper conductor, the main characteristics of which are summarized in Table I.

TABLE I
CONDUCTOR DIMENSIONS AND CHARACTERISTICS

Characteristic	Value
Effective copper cross section [mm^2]	70
Outer conductor diameter [mm]	9.5
Copper resistivity 20ºC [Ohm·m]	$1.85 \cdot 10^{-8}$
Temperature coefficient of resistance [K^{-1}]	0.0043
Number of strands [-]	14
Conductor mass per unit length [kg/m]	0.584
Ambient temperature [ºC]	12

Fig. 4 shows the temperature dependence of the specific heat of copper [29], which is used to calculate (9) and (11). It can be seen that in the range between 273 K and 500 K the specific heat of copper increases almost linearly with temperature.
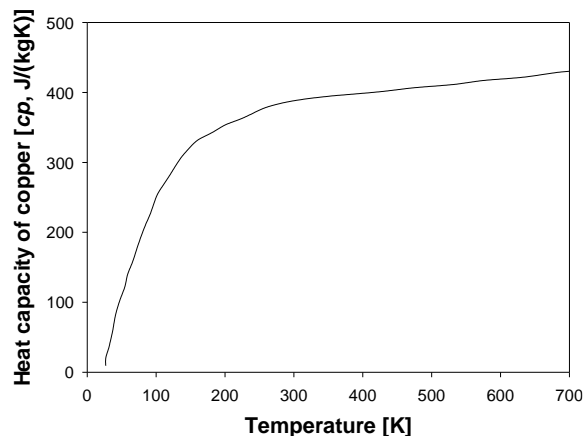

Fig. 4. Temperature evolution of the specific heat *cp* of copper [29].

B. Experimental results

In order to validate the thermal model of the conductor, the experimental short-circuit tests described in Table II were carried out. Experimental tests are the best tool to validate the accuracy of the equations developed in Section II and the FEM simulations. During these experimental tests, ambient temperature, electric current, and conductor temperature were measured according to the sampling frequencies described in Section IV.A.

TABLE II
SHORT-CIRCUIT TESTS CARRIED OUT

Test	RMS current [A]	Duration [s]
#1	6327	1.0
#2	6189	2.0
#3	5934	4.0
#4	5728	6.0

As shown in Table II, four experimental short-circuit tests were carried out in the laboratory with different current levels and short-circuit durations. They were carried out with the test setup shown in Fig. 2 using the copper conductor whose characteristics are summarized in Table I. The high-current transformer has a software program that allows the short-circuit duration to be selected and controls a fast electronic switch connected in series with the primary of the transformer. The current level is controlled by changing the voltage applied to the primary of the high-current transformer using an autotransformer. After each test, sufficient time was allowed for the conductor to return to the ambient temperature of the test area. The electrical resistance was measured before each test to check that its value had not changed using a Micro Centurion II micro ohmmeter from RayTech [30].

First, the different short-circuit tests described in Table II were simulated with the two simulation models, i.e., the three-dimensional FEM mode and the analytical model resulting from the solution of (9). The results are shown in Fig. 5.
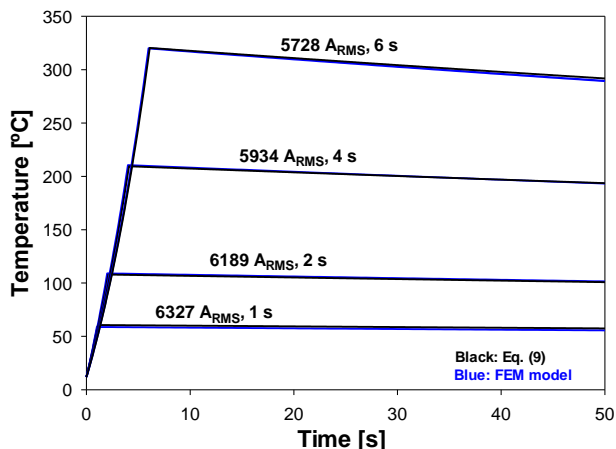
Fig. 5. Simulation results obtained with the analytical model given by (9) versus FEM simulations.

The results from Fig. 5 show equivalent results from both simulation models and therefore, due to the much reduced computational resources and much less computational time, i.e., 5000 s FEM simulation versus 0.030 s by applying (9) using an AMD Ryzen Threadripper 3960X 24-Core Processor, 3800 Mhz, with 48 GB RAM. Therefore, all simulation results presented from now on are based on solving (9) and (11). It should be noted that for more complex geometries the three-dimensional FEM model should be used.

Fig. 6 shows the temperature evolution of the conductor during the experimental short-circuit tests shown in Table II and the results of solving (9).
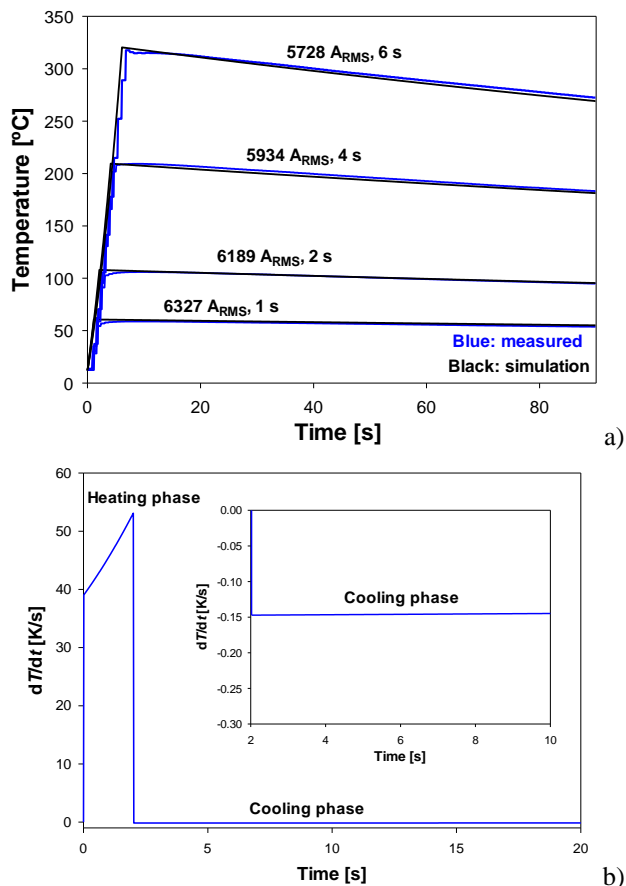

Fig. 6. Experimental versus simulation results. a) Temperature evolution of the conductor during the different short-circuit tests. b) Time derivative of the conductor temperature during the tests (short-circuit #2).

The results presented in Fig. 6a show the great similarity between experimental results and the simulations carried out by applying equations (1) – (9). It also shows a very different time derivative of the temperature during the heating and cooling phases of the short-circuit. Since the temperature rises much faster during the heating phase than it falls during the cooling phase, the adiabatic assumption is expected to apply. The results presented in Fig. 6 also show an almost linear decrease in temperature with time during the cooling phase of the short-circuit.

In order to better quantify the results presented in Fig. 6a, Table III shows the maximum experimental temperatures reached during the different short-circuit tests and those predicted by the simulation model.

TABLE III

MAXIMUM TEMPERATURES OF THE CONDUCTOR (DIAMETER = 9.5 MM) BASED ON EXPERIMENTS AND SIMULATIONS

#Test; RMS current, time	Maximum conductor temperature [ºC]		
	Simulation	Experimental	Difference
#1; 6327 A, 1s	60.64	58.7	3.24%
#2; 6189 A, 2s	107.9	105.9	1.89%
#3; 5934 A, 4s	209.4	209.3	0.05%
#4; 5728 A, 6s	319.8	317.7	0.79%

The results presented in Table III clearly show the accuracy of the transient thermal model of the conductor, since the maximum temperatures predicted by the model and the experimental ones are very similar. It should be noted that industrial short-circuit tests are usually limited to temperatures below 250 ºC [31], [32], so the model given by (9) has been tested beyond the requirements of the international standards.

In order to better understand the contributions of all terms in equation (3), Table IV shows their average values for short-circuit test #2. According to the results shown in Table IV, the heating rate is much higher than the cooling rate. Therefore, during the short-circuit duration (heating phase), the influence of the convective and radiative cooling terms is very small with respect to the $I^2_{RMS}R$ heating term.

TABLE IV

CONTRIBUTIONS OF THE HEATING AND COOLING TERMS IN (3) DURING SHORT-CIRCUIT TEST #2

Test phase	Heating term	Cooling terms	
	I_{RMS}^2R [W/m]	P_c [W/m]	P_r [W/m]
Heating phase (0-2 s)	11532.7	11.1	4.6

V. VALIDITY OF THE ADIABATIC ASSUMPTION DURING THE HEATING PHASE OF SHORT-CIRCUIT TESTS

Products intended for power applications are designed to safely withstand their rated short-circuit current without suffering mechanical damage. This section analyzes the validity of the adiabatic assumption to determine the maximum

temperature of the conductor during the short-circuit test. This is done based on the simulation model because of its high accuracy, which has been validated with experimental results. In order to validate the accuracy of the adiabatic approach, the results presented in this section assume a target temperature at the end of the short-circuit duration of 250 ºC, although some standards (e.g. IEC 62271-1 [3]) do not propose a specific maximum temperature at the end of the short-circuit.

A. Validity of the adiabatic approach

As explained, the adiabatic approach assumes no heat or mass transfer between the conductor and the environment. Therefore, convective and radiative cooling effects are neglected ($P_c = P_r = 0$) during the heating phase of the short-circuit. To validate the applicability of the adiabatic assumption, two types of simulations are carried out. The firsts are based on the full thermal model (non-adiabatic assumption), while the seconds neglect convective and radiative cooling effects. The results are summarized in Table V.

TABLE V
MAXIMUM CONDUCTOR TEMPERATURE (DIAMETER = 9.5 MM) BASED ON SIMULATIONS ASSUMING NON-ADIABATIC AND ADIABATIC CONDITIONS

#Test; RMS current, time	Maximum conductor temperature [ºC]		
	Non-adiabatic assumption (9)	Adiabatic assumption (11)	Difference
#1; 6327 A, 1s	60.64	60.67	0.05%
#2; 6189 A, 2s	107.9	108.0	0.09%
#3; 5934 A, 4s	209.4	210.1	0.14%
#4; 5728 A, 6s	319.8	322.2	0.62%

The results presented in Table V clearly show the validity of the adiabatic assumption of the short-circuit tests performed in this work.

Next, in order to determine the validity of the adiabatic assumption, several simulations are carried out assuming different short-circuit durations in which the maximum temperature of the conductor is 250 ºC, the practical limit suggested by some works [31], [32]. For this purpose, the current level in each simulation test is adjusted so that the maximum temperature of the conductor at the end of the heating phase of the short-circuit is 250 ºC. Simulations were carried out assuming short-circuit durations in the range of 2–20 seconds, considering adiabatic and non-adiabatic conditions, by applying equations (9) and (11), respectively. The results obtained are summarized in Table VI.

The results presented in Table VI show that the short-circuit can be extended up to 20 seconds in order to keep the temperature difference between non-adiabatic and adiabatic conditions below an arbitrary value of 5 ºC (2% difference with respect to 250 ºC).

TABLE VI
MAXIMUM CONDUCTOR TEMPERATURE (DIAMETER = 9.5 MM) BASED ON SIMULATIONS ASSUMING NON-ADIABATIC AND ADIABATIC CONDITIONS

Maximum conductor temperature [ºC]

Test conditions RMS current, time	Non-adiabatic assumption (9)	Adiabatic assumption (11)	Difference [ºC]
12824 A, 1 s	250.0	250.2	0.2
9073 A, 2 s	250.0	250.5	0.5
5246 A, 6 s	250.0	251.4	1.4
3718 A, 12 s	250.0	252.9	2.9
3042 A, 18 s	250.0	254.2	4.2
2884 A, 20 s	250.0	254.7	4.7
2640 A, 24 s	250.0	255.6	5.6

B. Validity of the adiabatic approach. Effect of the conductor radius

Since the heat is generated throughout the volume of the conductor and the cooling by radiation and convection is directly proportional to the surface area of the conductor as shown in (4) and (6), the smaller the ratio of surface area to volume of the conductor, the less heat it will lose relative to its volume, so that cooling is less effective for larger diameter conductors [33]. Therefore, the relative rate of cooling decreases as the radius of the conductor increases,

$$\frac{dT}{dt} \sim \frac{Area}{Volume} = \frac{2\pi r L}{\pi r^2 L} \sim \frac{1}{r} \tag{12}$$

According to (12), as the radius of the conductor increases, its volume increases faster than its surface area, so the cooling rate decreases and the adiabatic assumption should be more accurate. This is because the denominator in (12) controls the rate of heat generation while the numerator controls the rate of cooling (radiation and convection terms).

In this subsection a larger copper conductor is analyzed, the main parameters of which are summarized in Table VII.

TABLE VII
PARAMETERS OF THE COPPER CONDUCTOR WITH LARGER DIAMETER

Characteristic	Value
Effective copper cross section [mm^2]	185
Outer conductor diameter [mm]	15.3
Copper resistivity 20ºC [Ohm·m]	1.85·10^{-8}
Temperature coefficient of resistance [K^{-1}]	0.0043
Number of strands [-]	36
Conductor mass per unit length [kg/m]	1.521
Ambient temperature [ºC]	12

Simulations were then carried out using the copper conductor with a larger external diameter (15.3 mm instead of 9.5 mm), the results of which are shown in Table VIII. These simulations assume different durations for the heating phase of the short-circuit and the applied current is chosen so that the maximum temperature of the conductor at the end of the short-circuit is 250 ºC.

Comparing the results presented in Table VI (outer conductor diameter = 9.5 mm) with those presented in Table VIII (outer conductor diameter = 15.3 mm), it can be seen that the adiabatic approach is more accurate for larger conductors because the relative cooling rate decreases as the conductor diameter increases, as shown in (12). Therefore, for larger diameter conductors, the adiabatic approach can be applied for longer duration short-circuits. Furthermore, larger conductors have a lower resistance per unit length. These results suggest that if the temperature rise but not the mechanical behavior of the element under test is evaluated, short-circuit tests can be performed by

applying a reduced current at the expense of a longer short-circuit duration. This is very practical because it significantly reduces the instantaneous power and equipment requirements, allowing the use of less expensive equipment. For example, in the case of conductors with a diameter of 15.3 mm, the short-circuit duration can be up to 36 s, so in this case the short-circuit current is 5532.3 A compared to the 31924.4 A required for a 1 s short-circuit. Therefore, the current is reduced by a factor of 5.77, while the electrical power required is reduced by a factor of approximately $5.77^2 = 33.3$. For the cases analyzed and assuming a conductor of 1 m length, this means that the instantaneous power is reduced from approximately 200 kW to only 6 kW. It should be noted that these respective factors are not exactly 6 and 36, as it would be expected if $I^2_{RMS}t_{sc}$ were a constant value, mainly due to the temperature dependence of the resistance and specific heat of the conductor material, as well as the temperature dependence of the radiative and convective cooling terms. This approach opens up more possibilities, since the duration of the experimental short-circuit test could also be longer and thus the maximum temperature reached could be corrected by software.

TABLE VIII
MAXIMUM CONDUCTOR TEMPERATURE (DIAMETER = 15.3 MM) BASED ON SIMULATIONS ASSUMING NON-ADIABATIC AND ADIABATIC CONDITIONS

	Maximum conductor temperature [ºC]		
RMS current, time	Non-adiabatic test (9)	Adiabatic assumption (11)	Difference [ºC]
31924.4 A, 1 s	250.0	250.1	0.1
22944.5 A, 2 s	250.0	250.3	0.3
13404.2 A, 6 s	250.0	250.8	0.8
9517.0 A, 12 s	250.0	251.7	1.7
7787.5 A, 18 s	250.0	252.5	2.5
6755.5 A, 24 s	250.0	253.3	3.3
6051.5 A, 30 s	250.0	254.1	4.1
5532.3 A, 36 s	250.0	254.9	4.9

To better understand that the relative cooling rate decreases as the conductor diameter increases, Table IX analyzes the final temperature of two conductors of different sizes for the same test conditions (current level and short-circuit duration), assuming non-adiabatic and adiabatic conditions.

TABLE IX
MAXIMUM TEMPERATURES OF TWO CONDUCTORS (9.5 MM AND 15.3 MM DIAMETER) BASED ON SIMULATIONS ASSUMING NON-ADIABATIC AND ADIABATIC CONDITIONS

	Maximum conductor temperature [ºC]	
RMS current, time	Non-adiabatic/adiabatic Conductor 9.5 mm	Non-adiabatic/adiabatic Conductor 15.3 mm
12000 A,1 s	211.3/211.5	37.5/37.5
9000 A, 2 s	244.9/245.3	39.5/39.5
5000 A, 6 s	221.2/222.4	36.6/36.6
3500 A, 12 s	214.5/216.8	35.8/35.9
3000 A, 18 s	241.2/245.2	38.2/38.4
2500 A, 24 s	217.7/222.3	36.1/36.3

The results presented in Table IX show that the larger conductor heats up much less than the smaller one due to the difference in cross section. As expected, the temperature

difference between adiabatic and non-adiabatic conditions is always smaller for the larger conductor.

As an example, Table X shows the RMS value of the current required for the 15.3 mm conductor to reach 250 ºC assuming that $I^2_{RMS}t_{sc}$, also known as the Joule integral [34], is a constant value for different short-circuit durations, as well as the required current level in real environments, i.e., under non-adiabatic conditions.

TABLE X
CURRENT LEVEL REQUIRED FOR THE 15.3 MM CONDUCTOR TO REACH 250 ºC ASSUMING THAT $I^2_{RMS}t_{sc}$ IS A CONSTANT VALUE FOR DIFFERENT SHORT-CIRCUIT DURATIONS

	Applied RMS current [A]		Current ratio
Test duration t_{sc}	Adiabatic assumption (11)	Non-adiabatic test (Table 7)	$I_{non-adiabatic}/I_{adiabatic}$
1 s	31924.4	31924.4	1.000
2 s	22574.0	22944.5	1.016
6 s	13033.1	13404.2	1.028
12 s	9215.8	9517.0	1.033
18 s	7524.7	7787.5	1.035
24 s	6516.5	6755.5	1.037
30 s	5828.6	6051.5	1.038
36 s	5320.7	5532.3	1.040

It is possible to extend the short-circuit duration beyond the values given in Tables VIII and X. If the short-circuit duration is extended beyond the adiabatic limit, the maximum temperature reached at the end of the heating phase of the short-circuit would be lower than that reached in a standard short-circuit with a duration of 1 s and applying an equivalent $I^2_{RMS}t_{sc}$. Therefore, by applying (9) in the case of cylindrical samples or from FEM simulations for more complex geometries, it is possible to correct this temperature to match that of the standard short-circuit test.

VI. CONCLUSION

Standard short-circuit tests can only be performed in very specialized and expensive power laboratories due to the high electrical power and short duration current requirements, which are beyond the reach of the vast majority of electrical product manufacturers. This paper has analyzed the applicability of the adiabatic assumption in short-circuit testing. Adiabatic conditions assume that there is no heat or mass transfer between the conductor and the environment, so that convective and radiative cooling can be neglected, and it is assumed that all the heat generated during the short-circuit due to the Joule losses is completely used to raise the temperature of the conductor. This approach is of interest because it allows the duration of these tests to be increased with almost the same results, while the increased duration allows a large reduction in short-circuit current levels and instantaneous power requirements. This means that tests for product design, verification and quality control can be performed in a much less demanding and much more affordable laboratory, significantly reducing laboratory and testing costs. The maximum allowable temperature difference between non-adiabatic and adiabatic conditions depends on the expected temperature rise, customer requirements and the accuracy of the temperature sensors. In

general, a temperature rise of at least 250 °C is expected during the short circuit [35], so the allowable temperature difference could be set at around 5 °C, giving a relative temperature error of 2%. Based on this assumption, the paper has shown that reductions of six times the short-circuit current and about 36 times the required short-circuit power are possible by increasing the short-circuit duration. Even greater current reductions are possible by testing well beyond the adiabatic limit and applying the corrections proposed in this paper.

REFERENCES

[1] L. Gu *et al.*, "Analysis of Short-time Withstand Current and Peak Withstand Current Test of 500kV AC Fault Current Limiter," *Proc. 2021 IEEE 4th Int. Electr. Energy Conf. CIEEC 2021*, May 2021.

[2] C. Abomailek, J.-R. Riba, F. Capelli, and M. Moreno-Eguilaz, "Fast electro-thermal simulation of short-circuit tests," *IET Gener. Transm. Distrib.*, vol. 11, no. 8, pp. 2124–2129, Jun. 2017.

[3] N. Dorraki and K. Niayesh, "An Experimental Study of Short-Circuit Current Making Operation of Air Medium-Voltage Load Break Switches," *IEEE Trans. Power Deliv.*, 2022.

[4] A. Murzintsev, A. Korolev, K. Zhgun, and R. Baembitov, "Short-circuit Current Reduction in Auxiliary Network of Traction Substations," *Transp. Res. Procedia*, vol. 54, pp. 346–354, Jan. 2021.

[5] F. Capelli, J.-R. Riba, D. González, and D. Gonzalez, "Optimization of short-circuit tests based on finite element analysis," in *2015 IEEE International Conference on Industrial Technology (ICIT)*, 2015, vol. 2015-June, no. June, pp. 1368–1374.

[6] J. Schlabbach and K. H. Rofalski, *Power System Engineering: Planning, Design, and Operation of Power Systems and Equipment*. Weinheim, Germany: WILEY-VCH Verlag GmbH & Co., 2008.

[7] H. Li, A. Bose, and Y. Zhang, "On-line short-circuit current analysis and preventive control to extend equipment life," *IET Gener. Transm. Distrib.*, vol. 7, no. 1, pp. 69–75, Jan. 2013.

[8] M. Tartaglia and M. Mitolo, "An Analytical Evaluation of the Prospective I2t to Assess Short-Circuit Capabilities of Cables and Busways," *IEEE Trans. Power Deliv.*, vol. 25, no. 3, pp. 1334–1339, Jul. 2010.

[9] H. Wu, L. Yuan, L. Sun, and X. Li, "Modeling of Current-Limiting Circuit Breakers for the Calculation of Short-Circuit Current," *IEEE Trans. Power Deliv.*, vol. 30, no. 2, pp. 652–656, Apr. 2015.

[10] M. P. Filippakou, C. G. Karagiannopoulos, D. P. Agoris, and P. D. Bourkas, "Electrical contact overheating under short-circuit currents," *Electr. Power Syst. Res.*, vol. 57, no. 2, pp. 141–147, 2001.

[11] IEC, "IEC TR 60909-1:2002. Short-circuit currents in three-phase a.c. systems - Part 1: Factors for the calculation of short-circuit currents according to IEC 60909-0." IEC, Geneva, Switzerland, p. 170, 2002.

[12] International Electrotechnical Commission, "IEC 62271-1:2017. High-voltage switchgear and controlgear - Part 1: Common specifications for alternating current switchgear and controlgear." International Electrotechnical Commission, p. 260, 2017.

[13] International Electrotechnical Commission, "IEC-60694. Common specifications for high-voltage switchgear and controlgear standards." IEC, Geneva, Switzerland, p. 234, 2002.

[14] "ANSI C37.51a-2010 Switchgear - Metal-Enclosed Low-Voltage AC Power Circuit Breaker Switchgear Assemblies -Conformance Test Procedures." [Online]. Available: http://webstore.ansi.org/RecordDetail.aspx?sku=ANSI+C37.51a-2010. [Accessed: 31-Oct-2015].

[15] IEEE, "IEEE Std C37.20.1-2015 (Revision of IEEE Std C37.20.1-2002). IEEE Standard for Metal-Enclosed Low-Voltage (1000 Vac and below, 3200 Vdc and below) Power Circuit Breaker Switchgear," *IEEE Std C37.20.1-2015 (Revision of IEEE Std C37.20.1-2002)*. IEEE, pp. 1–84, 2015.

[16] Y. Fan, X. Wen, and S. A. K. S. Jafri, "3D transient temperature field analysis of the stator of a hydro-generator under the sudden short-circuit condition," *IET Electr. Power Appl.*, vol. 6, no. 3, p. 143, 2012.

[17] T.-H. Chen and R.-N. Liao, "Modelling, simulation, and verification for detailed short-circuit analysis of a 1 × 25 kV railway traction system," *IET Gener. Transm. Distrib.*, vol. 10, no. 5, pp. 1124–1135, Apr. 2016.

[18] F. Capelli, J.-R. Riba, and J. Pérez, "Three-Dimensional Finite-Element Analysis of the Short-Time and Peak Withstand Current Tests in Substation Connectors," *Energies*, vol. 9, no. 6, p. 418, May 2016.

[19] S. S. M. Ghoneim, M. Ahmed, and N. A. Sabiha, "Transient Thermal Performance of Power Cable Ascertained Using Finite Element Analysis," *Process. 2021, Vol. 9, Page 438*, vol. 9, no. 3, p. 438, Feb. 2021.

[20] G. Liu, W. Zheng, D. Guo, R. Peng, X. Lin, and M. Zhong, "Numerical modeling and analysis of thermal and mechanical behavior for ground wire-clamp system under short-circuit current," *Electr. Power Syst. Res.*, vol. 201, p. 107497, Dec. 2021.

[21] A. Cocchi, G. De Marzi, A. Lampasi, and R. Romano, "Electrothermal design of DC busbars for fusion facilities," *Fusion Eng. Des.*, vol. 170, p. 112662, Sep. 2021.

[22] IEEE Std 738-2012, "IEEE Standard for Calculating the Current-Temperature of Bare Overhead Conductors," New York, USA, 2012.

[23] Cigré Working Group 22.12, "Thermal behaviour of overhead conductors," Cigré, Paris (France), 2002.

[24] J. Golebiowski and M. Zareba, "Temperature-time profiles of a tubular bus in shorting conditions," *Przegląd Elektrotechniczny*, vol. R. 96, nr 3, no. 3, pp. 146–149, 2020.

[25] R. Wilkins, T. Saengsuwan, and L. O'Shields, "Short-circuit tests on current-limiting fuses: modelling of the test circuit," *Gener. Transm. Distrib. IEE Proc. C*, vol. 140, no. 1, pp. 30–36, Jan. 1993.

[26] S. Victoria Mary and C. Pugazhendhi Sugumaran, "Investigation on magneto-thermal-structural coupled field effect of nano coated 230 kV busbar," *Phys. Scr.*, vol. 95, no. 4, p. 045703, Feb. 2020.

[27] Ľ. Beňa *et al.*, "Calculation of the overhead transmission line conductor temperature in real operating conditions," *Electr. Eng.*, vol. 103, no. 2, pp. 769–780, 2021.

[28] S. S. Hong *et al.*, "Internet of Things-Based Monitoring for HV Transmission Lines: Dynamic Thermal Rating Analysis with Microclimate Variables," *2020 8th Int. Electr. Eng. Congr. iEECON 2020*, Mar. 2020.

[29] B. Banerjee, "An evaluation of plastic flow stress models for the simulation of high-temperature and high-strain-rate deformation of metals," *Acta Mater.*, vol. 58, no. 20, pp. 6810–6827, Dec. 2005.

[30] J. Martinez, A. Gomez-Pau, J.-R. Riba, and M. Moreno-Eguilaz, "On-Line Health Condition Monitoring of Power Connectors Focused on Predictive Maintenance," *IEEE Trans. Power Deliv.*, pp. 1–1, Dec. 2020.

[31] Domingo; J.M., "Study of the behaviour of a n-metal cable screen subject to an adiabatic short-circuit," in *9th International Conference on Insulated Power Cables, JiCable'15*, 2015, pp. 1–4.

[32] C. H. Bonnard, A. Blavette, S. Bourguet, and A. Charmetant, "Modeling of a wave farm export cable for electro-thermal sizing studies," *Renew. Energy*, vol. 147, pp. 2387–2398, Mar. 2020.

[33] G. Planini and M. Vollmer, "The surface-to-volume ratio in thermal physics: from cheese cube physics to animal metabolism," *Eur. J. Phys.*, vol. 29, no. 2, p. 369, Feb. 2008.

[34] M. Mitolo and M. Tartaglia, "An analytical evaluation of the factor k2 for protective conductors," *Conf. Rec. - IAS Annu. Meet. (IEEE Ind. Appl. Soc.*, 2011.

[35] IEC, "IEC 61238-1-1:2018 Compression and mechanical connectors for power cables - Part 1-1: Test methods and requirements for compression and mechanical connectors for power cables for rated voltages up to 1 kV (Um = 1,2 kV) tested on non-insulated conductors." IEC, Geneva, Switzerland, pp. 1–89, 2018.